Hydrodynamic interactions in DNA thermophoresis

Aboubakry Ly, Aloïs Würger

Hydrodynamic interactions in DNA thermophoresis

Aboubakry Ly and Alois Würger
Laboratoire Ondes et Matière d'Aquitaine, Université de Bordeaux & CNRS, 33405 Talence, France

We theoretically study the molecular-weight dependence of DNA thermophoresis, which arises from mutual advection of the n repeat units of the molecular chain. As a main result we find that the dominant driving forces, i.e., the thermally induced permittivity gradient and the electrolyte Seebeck effect, result in characteristic hydrodynamic screening. In comparison with recent experimental data on single-stranded DNA ($2 \leq n \leq 80$), our theory quantitatively describes the increase of the drift velocity up to $n = 30$; the slowing-down of longer molecules is well accounted for by a simple model for counterion condensation. It turns out that thermophoresis may change sign as a function of n: For an appropriate choice of the salt-specific Seebeck coefficient, short molecules move to the cold and long ones to the hot; this could be used for separating DNA by molecular weight.

PACS numbers:

When applying a temperature gradient on a colloidal dispersion, one observes thermally driven transport towards the hot or the cold [1, 2]. In recent years, thermophoresis has been shown to provide a versatile means for manipulating DNA, including translocation through plasmonic nanopores [3], stretching in nanochannels [4, 5], separation by molecular weight [6], sequence-specific detection with functionalized nanoparticles [7], and force-free trapping of single molecules [8]. Protein thermophoresis has become a standard technology in biomedical analysis [9], and the accumulation of RNA in hydrothermal pores is discussed as a scenario for biomolecular synthesis in the early evolution of life [10].

In the last decade, much progress has been made concerning the physical mechanisms of thermophoresis of charged colloids. It has been shown that, in addition to thermo-osmosis [11, 12], the electrolyte Seebeck field [13–18] and concentration gradients of salt [16] or nonionic polymers [19, 20], play an important role. These companion fields arise from specific solvation enthalpies of salt ions or nonionic solutes, and are at the origin of the "inverse" Soret effect, where the colloids accumulate in hot regions [16, 19]. Regarding the size dependence, there is conclusive evidence that the mobility of colloidal beads does not vary with the radius [21, 22].

In spite of the many experimental studies mentioned above, little is known on the molecular-weight dependence of DNA thermophoresis. If the hydrodynamic slowing-down of Brownian motion is well understood in terms of mutual advection of the repeat units [23], a more complex picture arises for phoretic motion where external forces are absent and which is driven by non-equilibrium surface properties. For short-ranged dispersion forces, hydrodynamic interactions are irrelevant and the thermophoretic velocity is constant [24, 25]; deviations observed for very short polymers in organic solvents [26], arise probably from chemically different end groups. For DNA in a weak electrolyte, however, the electrostatic interaction length may attain tens of nanometers, which suggests an incomplete screening of hydrodynamic coupling.

In this paper we study hydrodynamic effects on DNA thermophoresis. We consider the two dominant charge-related surface forces, i.e., the thermally induced permittivity gradient and the electrolyte Seebeck effect, and derive the respective hydrodynamic correction factors in the rigid-rod limit. With a simple model for counterion condensation, we compare our theory to recent Soret data for single-stranded DNA [17].

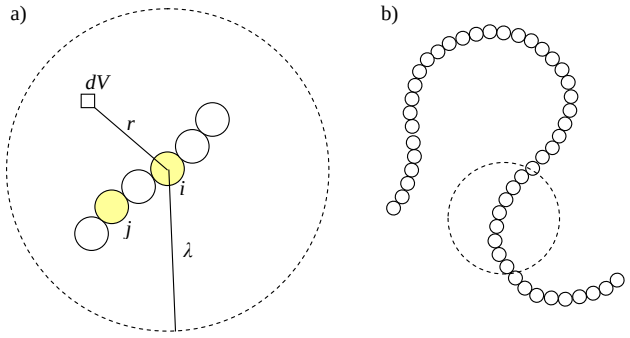

FIG. 1: Schematic view of a charged polymer in an electrolyte solution. a) The drag on the molecular unit j consists of two contributions: First, the stokeslet of bead i, driven by the force $\mathbf{F}$, drags the neighbor j. Second, due to the force $\mathbf{f}(\mathbf{r})$ exerted by the bead i, the fluid element dV moves and in turn exerts a drag on bead j. These contributions cancel each other at distances well beyond the Debye length λ. b) Since the persistence length is of the order of the Debye length, the molecule may be treated as a rigid rod within the reach of electrostatic interactions.

Hydrodynamic interactions. – Consider a polyelectrolyte chain of n building blocks, as illustrated in Fig. 1. Unit i creates a flow field $\mathbf{v}(\mathbf{r}-\mathbf{r}_i)$ in the surrounding fluid and thus drags its neighbor j. Then the overall velocity $\mathbf{u}$ of the chain is given by the sum of the monomer contribution $\mathbf{u}_1$ and the mutual advection,

$$\mathbf{u} = \mathbf{u}_1 + \frac{1}{n}\sum_{i,j\neq i} \langle \mathbf{v}(\mathbf{r}_{ij})\rangle \,, \tag{1}$$

where the angular brakets $\langle\cdots\rangle$ indicates the configurational average with respect to $\mathbf{r}_{ij} = \mathbf{r}_j - \mathbf{r}_i$.

Thermophoresis arises from the solute-solvent interactions. The force density exerted on the counterion cloud surrounding a charged monomer reads as [27]

$$\mathbf{f} = -\frac{E^2}{2}\nabla\epsilon + \rho\mathbf{E}_T, \tag{2}$$

where the first term is proportional to the thermally induced permittivity gradient $\nabla\epsilon = (d\epsilon/dT)\nabla T$, with the charged monomer's electric field E. Since the permittivity decreases with rising temperature, $d\epsilon/dT < 0$, the surrounding water moves to the hot, as recently confirmed experimentally for thermoosmosis in a capillary [12]. By reaction, the molecule migrates toward the cold.

The second term in (2) describes the force exerted by the macroscopic thermoelectric field $\mathbf{E}_T = S\nabla T$ on the monomer's counterion density ρ [14]. The electrolyte Seebeck coefficient S is a salt-specific quantity that may take either sign, resulting in motion along the temperature gradient or opposite to it [16]. Eq. (2) gives the dominant thermal forces to leading order in the ratio a/λ of the monomer radius and the Debye length. Additional companion fields, such as the salinity gradient, arise in the colloid limit where a is comparable to or larger than λ [16].

The force density $\mathbf{f}$ acts on the surrounding water and, by reaction, the molecular unit is subject to the opposite force $\mathbf{F} = -\int dV\mathbf{f}$ [27]. Thus the velocity field induced by the moving bead i at the position of its neighbor j, consists of two contributions,

$$\mathbf{v}(\mathbf{r}_{ij}) = \mathbf{G}(\mathbf{r}_{ij})\cdot\mathbf{F} + \int \mathbf{G}(\mathbf{r}_{ij}-\mathbf{r})\cdot\mathbf{f}(\mathbf{r})dV, \tag{3}$$

where $\mathbf{G}(\mathbf{r}) = (1+\widehat{\mathbf{r}}\widehat{\mathbf{r}})/8\pi\eta r$ is the Oseen tensor with the viscosity η and $\widehat{\mathbf{r}} = \mathbf{r}/r$ [28]. The first term describes the long-range velocity field $v \sim 1/r_{ij}$ or "stokeslet" of particle i at the position j, due to the force $\mathbf{F}$; it gives rise to strong hydrodynamic effects on diffusion and sedimentation [23]. The second term is characteristic for phoretic motion; it may be viewed as the sum of stokeslet flows of strength $\mathbf{f}dV$ and centered at a distance $\mathbf{r}$ from particle i, as illustrated in Fig. 1a. Since both E and ρ vanish well beyond the Debye length, the second term cancels the first one at large distances, $r_{ij} \gg \lambda$, whereas it is small for nearby beads.

As a consequence of this hydrodynamic screening, the advection velocity (3) varies as $1/r_{ij}$ within the Debye length but vanishes at larger distances. When performing the configurational average in (1) with the (isotropic) equilibrium distribution function, the only finite component of the mean drag velocity is along the force density $\mathbf{f}$, that is, along the temperature gradient. Then the tensor equation simplifies to a scalar one, and Eq. (1) becomes

$$u = u_1 + \frac{1}{n}\sum_{i,j\neq i}\int \langle G(|\mathbf{r}_{ij}-\mathbf{r}|) - G(r_{ij})\rangle f(\mathbf{r})dV, \tag{4}$$

with the Oseen tensor replaced by its diagonal part $G(r) = 1/6\pi\eta r$. This form shows that mutual advection vanishes for distant pairs with $r_{ij} \gg \lambda$, thus nicely displaying hydrodynamic screening.

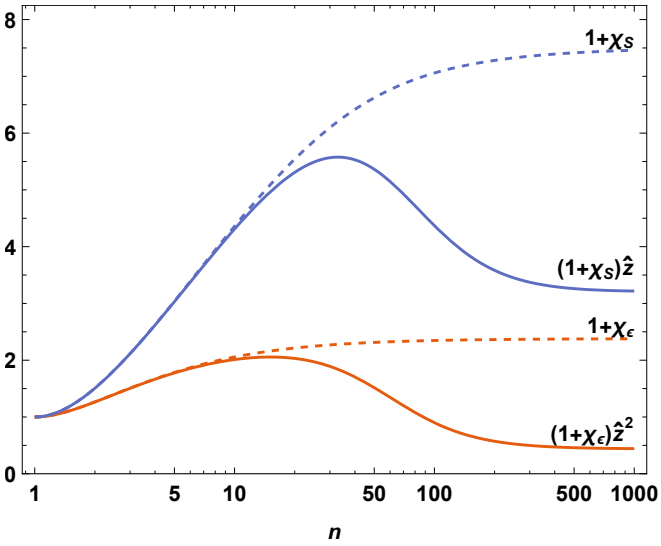

FIG. 2: Molecular-weight dependence of the two contributions to D_T. Both hydrodynamic factors χ_ϵ and χ_S increase with n, albeit with differnt amplitudes, as shown by the dashed lines; the parameters are the monomer distance $d = 3$Å and the Debye length $\lambda = 5$ nm. Counterion condensation results in the factors $\hat{z}^2$ and $\hat{z}$, which significantly reduce the mobility (solid lines), according to (9) with $\beta_n = (n^2-1)n_0^{-2}$ and $n_0 = 80$.

In order to evaluate (4) we need to explicit the force density $f(\mathbf{r})$. The electrostatic potential of a single bead of valency $\hat{z}$ is well described by the Debye-Hückel expression

$$\psi = -\frac{\hat{z}e}{4\pi\epsilon r}e^{-r/\lambda} = \zeta_1\frac{a}{r}e^{-r/\lambda}, \tag{5}$$

where the second equality defines the single-bead surface potential $\zeta_1 = -\hat{z}e/4\pi\epsilon a$, which we assume to be negative. One readily obtains the radial electric field $E = -d\psi/dr$ and the counterion charge density $\rho = -\epsilon\psi/\lambda^2$ which determine the force density (2). Then the volume integrals in (4) can be performed in closed form [29], resulting in the factors $\langle e^{-2r_{ij}/\lambda}/r_{ij}^2\rangle$ and $\langle e^{-r_{ij}/\lambda}/r_{ij}\rangle$. Since the main contribution to Eq. (4) stems from within the screening length λ, which in turn is comparable to the molecular persistence length [30], the chain may be treated as rigid such that the distance of beads i, j simplifies to $r_{ij} = |i-j|\,d$. Replacing moreover the double sum by integrals over i and j, we obtain

$$\mathbf{u} = \frac{\zeta_1^2}{3\eta}(1+\chi_\epsilon)\nabla\epsilon + \frac{2\epsilon\zeta_1}{3\eta}(1+\chi_S)\mathbf{E}_T, \tag{6}$$

where the quantities χ_ϵ and χ_S account for hydrodynamic interactions (see Fig. 2.) With $\chi_\epsilon = 0 = \chi_S$ one has the explicit expression for the monomer velocity $\mathbf{u}_1$ defined in (1).

The hydrodynamic correction factor for motion driven by the permittivity gradient reads

$$\chi_\epsilon = \frac{a^2}{d^2}\left((1+2n\hat{d})\frac{E_{2\hat{d}}-E_{2n\hat{d}}}{n}+e^{-2\hat{d}}-\frac{e^{-2n\hat{d}}}{n}\right), \quad (7)$$

with the shorthand notation $E_x = \mathrm{Ei}(-x)$ for the exponential integral function, and $\hat{d} = d/\lambda$ for the ratio of the monomer length and the Debye length. For the Seebeck term we find

$$\chi_S = \frac{2a}{d}\left(E_{n\hat{d}} - E_{\hat{d}} + \frac{e^{-n\hat{d}}-e^{-\hat{d}}}{n\hat{d}}\right), \quad (8)$$

The factor 2 in the exponential and Ei functions in χ_ϵ arises from the screening factor of the force density, $E^2 \propto e^{-2r/\lambda}$, whereas the factors in χ_S are related to the decay of the screening cloud, $\rho \propto e^{-r/\lambda}$. Fig. 2 shows χ_ϵ and χ_S as a function of the molecular weight. Both vanish for monomers, $n = 1$, whereas for long molecules they tend toward the constants $\chi_\epsilon^\infty = (a/d)^2(2\hat{d}E_{2\hat{d}} + e^{-2\hat{d}})$ and $\chi_S^\infty = -2(a/d)E_{\hat{d}}$. Note that χ_S is identical to the hydrodynamic correction of electrophoresis [31]. Flexible molecules with a power law $\langle r_{ij}^2\rangle \propto |i-j|^{2\nu}$, would result in cumbersome expressions with the incomplete Gamma function $\Gamma(\nu^{-1}, nd/\lambda)$ instead of the exponential integral function, without changing the qualitative features.

Counterion condensation.– A polyelectrolyte carries a line charge e/d. If the bead spacing d is larger than the Bjerrum length $l_B \approx 7$Å, Debye-Hückel approximation is valid even for long chains, and the electrostatic potential reads $\sum_i \psi_i(\mathbf{r}-\mathbf{r}_i)$. Yet in the opposite case $d < l_B$, which is relevant for DNA, this linear superposition ceases to be valid as n increases. Because of the strong Coulomb interaction, the counterions partly condense onto the polymer until its linear charge density is reduced to the critical value e/l_B [32]. The remaining free counterions are well described by Debye-Hückel theory.

In a mean-field model, counterion condensation is described by an effective valency

$$\hat{z} = \xi^{-1} + \frac{1-\xi^{-1}}{1+\beta_n}, \quad (9)$$

where $\xi = l_B/d > 1$ is the Manning parameter. For a monomer the quantity β_1 vanishes, and one has $\hat{z} = 1$. For long chains, β_n tends to infinity, thus resulting in $\hat{z} = \xi^{-1}$ and reducing the charge density to its critical value $\hat{z}e/d = e/l_B$ [32]. The progressive condensation of the counterions on the chain, and the dependence of β_n on n and λ, constitute an intricate problem which is beyond the scope of the present paper [33]. Here we use the simple form $\beta_n = (n^2-1)n_0^{-2}$ which, with $n_0 = 80$, fits rather well the experimental data. Note that this model does not depend on the electrolyte strength.

Phoretic coefficients.– The thermophoretic mobility is defined through the drift velocity $u = -D_T\nabla T$ in a temperature gradient. From (6) we find

$$D_T = \frac{k_B}{12\pi\eta a}\left(\frac{l_B}{a}\hat{z}^2(1+\chi_\epsilon)\tau + 2\hat{z}(1+\chi_S)\hat{S}\right), \quad (10)$$

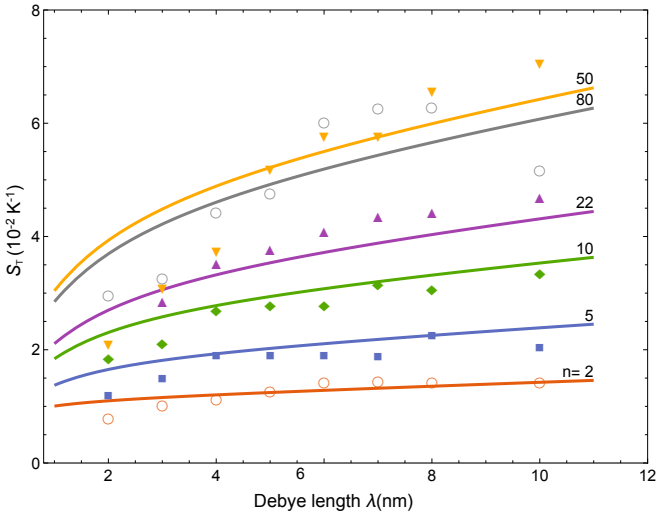

FIG. 3: The Soret coefficient S_T as a function of the Debye length λ for DNA of different length n. The data points, measured at 15° C, are taken from Ref. [17]. The theory curves are calculated from $S_T = D_T/D$, where D_T is given by Eq. (10) with $\hat{S} = 0$, $a = 4.25$Å, and $d = 3$Å. The values of the diffusion coeffcient D are shown in the inset; those for $n = 5, ..., 50$ are measured [17], that for $n = 2$ is extrapolated from the previous, and the one at $n = 80$ corresponds to the known power law for long molecules [35].

with the parameter $\tau = -d\ln\epsilon/d\ln T \approx 1.4$ which arises from the permittivity gradient, and the dimensionless Seebeck coefficient $\hat{S} = S(e/k_B)$. For monomers the mobility is independent of the Debye length, whereas for longer chains, the correction factors give rise to complex dependencies on λ and n. In Fig. 2 we plot the two contributions to D_T as a function of n. The initial increase results from hydrodynamic interactions (dashed lines), whereas the decrease at larger n is due to counterion condensation (solid lines). Both factors reach a finite value at large n; for typical parameters of DNA in a weak electrolyte, the permittivity term shows an overall decrease, $\hat{z}^2(1+\chi_\epsilon^\infty) < 1$, whereas the Seebeck term is enhanced, $\hat{z}(1+\chi_S^\infty) > 1$.

The stationary DNA concentration c is achieved when thermophoretic drift and gradient diffusion with coefficient D cancel each other, $cu - D\nabla c = 0$. This "Soret equilibrium" is usually written in the form $\nabla c + cS_T\nabla T = 0$, since experiments probe the Soret coefficient $S_T = D_T/D$ rather than the mobility D_T. In Fig. 3 we compare our theory with Soret data for single-stranded DNA as a function of the Debye length λ, taken from Ref. [17]. The theoretical curves are calculated with (10) and a simple model for the measured diffusion coefficient D, as described in [29]. The best agreement with the data is obtained when retaining in (10) the permittivity-gradient term only, that is, for zero Seebeck coefficient, $\hat{S} = 0$. The increase of S_T with the Debye length arises mainly from the hydrodynamic correction χ_ϵ. For short chains, $n < 30$, the variation with n is of purlely hydrodynamic

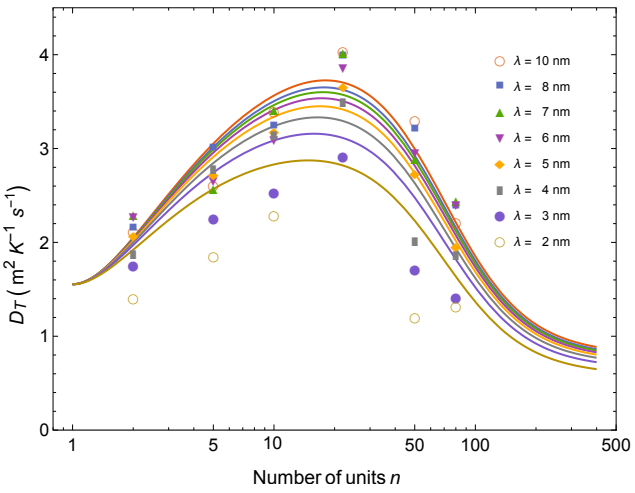

FIG. 4: Thermophoretic mobility D_T as a function of the molecular length n for three values of the Debye length λ. The full curves are calculated from Eq. (10) with $\hat{S} = 0$, $a = 4.25$Å and $d = 3$Å. The data points give $D_T = DS_T$, with S_T and the hydrodynamic radius from Ref. [17]; for details see [29].

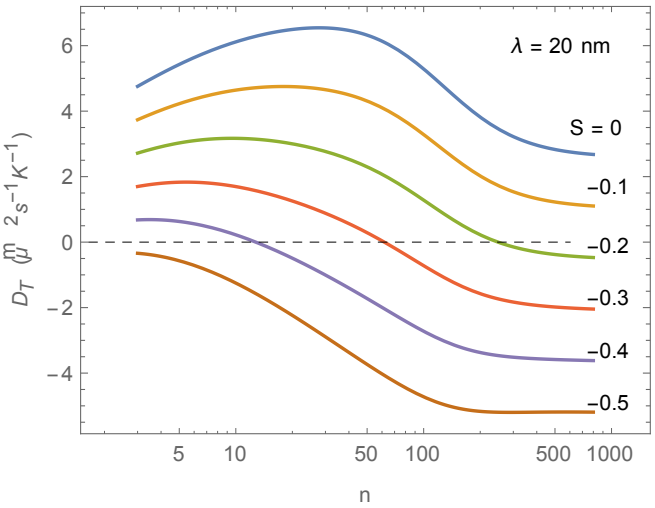

FIG. 5: Thermophoretic mobility D_T as a function of the chain length n, for different values of the dimensionless Seebeck coefficient $\hat{S}$. For negative $\hat{S}$ the thermoelectric field in (6) drives the molecules toward the hot, whereas the permittivity gradient points toward the cold. Since the latter dominates for short molecules and the latter for long ones, D_T changes sign as the n increases.

origin, whereas for larger chains counterion condensation plays an important role, as is clear from Fig. 2.

In order to clearly display the effect of hydrodynamic interactions, we plot in Fig. 4 the thermophoretic mobility (10) as a function of the molecular weight n. The experimental points are obtained from $D_T = DS_T$, with measured S_T and D [17] as described in Fig. [29]. The theoretical curves are calculated with the permittivity-gradient only ($\hat{S} = 0$). The initial increase of the data up to $n = 22$ agree quantitatively with the relation (7), thus providing strong evidence for the role of hydrodynamic interactions. The maximum and the subsequent decrease are well described by counterion condensation according to (9). Adding a significant thermoelectric contribution would not improve the quality of the fit, quite on the contrary. This suggests that the Seebeck field in NaCl solution is small, confirming a previous analysis of Soret data for polystyrene beads [16].

The electrolyte Seebeck effect was discarded in the above analysis of Soret data in NaCl solution. In Fig. 5 we plot the complete mobility D_T as a function of n, for several values of the dimensionless Seebeck coefficient $\hat{S}$. As the most striking feature, for negative $\hat{S}$ the superposition of the two contributions in (10) may result in a change of sign of the D_T. From Fig. 2 it is clear that for short chains, the permittivity gradient term prevails, whereas for longer moleculese the Seebeck term dominates because of its much larger hydrodynamic factor χ_S.

The resulting velocity difference could be used for specific accumulation of one component at a heated spot, or for separating DNA by molecular size. For example, in an electrolyte with $\hat{S} = -0.3$, the permittivity-gradient term dominates for short molecules ($n < 50$) which move to the cold accordingly, whereas longer chains ($n > 50$) are driven to the hot by the thermoelectric field E_T. The stagnation molecular length n_c, where $D_T = 0$, is easily adapted by chosing an appropriate salt mixture. The change of sign has been observed for nano-size micelles [15] and micron-size polystyrene beads [16] in mixed electrolytes $NaOH_xCl_{1-x}$; the values of $\hat{S}$ used in Fig. 5 are realized by with $0.1 < x < 0.4$.

Conclusion. – We briefly summarize our main results on DNA thermophoresis. First, D_T does not vanish in the limit of high salinity or small Debye length, contrary to what is known for micron-size colloidal particles [16] and what was assumed to hold true for DNA: A finite value for small λ was observed in a recent experiment [17], and interpreted as a non-ionic contribution due to dispersion forces. In our Eq. (10) this limit is obtained by letting $\chi \to \chi^\infty$ and $\hat{z} \to \xi^{-1}$, revealing the existence of a large residual double-layer contribution.

Second,we find that DNA thermophoresis is rather sensitive to hydrodynamic interactions. With increasing chain length n, the mobility is enhanced due to mutual advection of the repeat units, then passes through a maxium, and finally decreases below the monomer value due to counterion condensation. Comparison with measured data in Fig. 4, provides strong evidence that the molecular-weight dependence arises from the interplay of hydrodynamic interactions and non-linear charge effects.

Fourth, the interplay between the dominant driving forces, that is, the permittivity gradient and a thermoellectric field with negative Seebeck coefficient, results in a change of sign as a funciton of n: Short molecules move

to the cold, and long ones to the hot.

The authors acknowledge funding by Agence Nationale de la Recherche through contract ANR-13-IS04-0003.

[1] R. Piazza, Soft Matter **4**, 1740 (2008).
[2] A. Würger, Rep. Prog. Phys. **73**, 126601 (2010)
[3] F. Nicoli, D. Verschueren, M. Klein, C. Dekker, and M.P. Jonsson, Nano Lett. **14**, 6917 (2014)
[4] J.N. Pedersen, C.J. Lüscher, R. Marie, L.H. Thamdrup, A. Kristensen, and H. Flyvbjerg, Rev. Lett. **113**, 268301 (2014)
[5] Y. He, M. Tsutsui, R.H. Scheicher, F. Bai, M. Taniguchi, and T. Kawai, ACS Nano **7,** 538 (2013)
[6] Y.T. Maeda, A. Buguin, and A. Libchaber, Phys. Rev. Lett. **107,** 038301 (2011)
[7] L.-H. Yu and Y.-F. Chen, Anal. Chem. **87**, 2845 (2015)
[8] M. Braun, T. Thalheim, K. Günther, M. Mertig, and F. Cichos, Proc. SPIE 9922, Optical Trapping and Optical Micromanipulation XIII, 99220Z (2016)
[9] M. Jerabek-Willemsen, T. Andréa, R. Wannera, H.M. Rotha, S. Duhr, Ph. Baaske, D. Breitsprecher, J. Mol. Structure **1077,** 101 (2014)
[10] P. Baaske, F.M. Weinert, S. Duhr, K.H. Lemke, M.J. Russell, and D. Braun, PNAS **104**, 9346 (2007)
[11] E. Ruckenstein, J. Coll. Interf. Sci. **83**, 77 (1981)
[12] A.P. Bregulla, A. Würger, K. Günther, M. Mertig, and F. Cichos, Phys. Rev. Lett. **116**, 188303 (2016)
[13] S.A. Putnam, D.G. Cahill, G.C.L. Wong, Langmuir **23**, 9221 (2007)
[14] A. Würger, Phys. Rev. Lett. **101**, 108302 (2008)
[15] D. Vigolo, S. Buzzaccaro and R. Piazza, Langmuir **26**, 7792 (2010).
[16] K.A. Eslahian, A. Majee, M. Maskos, A. Würger, Soft Matter **10**, 1931 (2014)
[17] M. Reichl, M. Herzog, A. Götz, and D. Braun, Phys. Rev. Lett. **112**, 198101 (2014)
[18] S. Simoncelli, J. Summer, S. Nedev, P. Kühler, and J. Feldmann, Small **29**, 2854 (2016).
[19] H.-R. Jiang, H. Wada, N. Yoshinaga and M. Sano, Phys. Rev. Lett. **102**, 208301 (2009)
[20] T. Tsuji, K. Kozai, H. Ishino, and S. Kawano, Micro & Nano Letters, doi: 10.1049=mnl.2012.0357 (2017)
[21] M. Braibanti, D. Vigolo, R. Piazza, Phys. Rev. Lett. **100**, 108303 (2008).
[22] A. Würger, Phys. Rev. Lett. **116**, 138302 (2016)
[23] P. -G. de Gennes, Scaling concepts in Polymer Physics, Cornell University Press: Ithaca (1979)
[24] F. Brochard, P.-G. de Gennes, C. R. Acad. Sc. Paris, Série II **293**, 72 (1981)
[25] S. Wiegand, J. Phys. Cond. Matt. **16**, 357 (2004)
[26] D. Stadelmaier, W. Köhler, Macromolecules **41**, 6205 (2008)
[27] J. Morthomas and A. Würger, Eur. Phys. J. **27**, 425-434 (2008)
[28] S. Kim, S. J. Karilla, Microhydrodynamic: Principles and Selected Applications, Butterworth-Heinemann Boston (1991)
[29] Details for the derivation of the thermophoretic mobility, the effective charge, and the experimental data and graphs are given in Supplementary Material.
[30] B. Tinland, A. Pluen, J. Sturm, and G. Weill, Macromolecules **30**, 5763 (1997)
[31] M. Muthukumar, Macro. Theo. Simul. **3,** 61-71 (1994)
[32] G. S. Manning, J. Chem. Phys. **51**, 924 (1969) and J. Phys. Chem. **85,** 1508-1515 (1981)
[33] K. Grass and C. Holm, Faraday Discuss. **144**, 57-70 (2010)
[34] See Supplemental material for technical details
[35] A. Sim, J. Lipfert, D. Herschlag, S. Doniach, Phys. Rev. E. **86,** 021901 (2012)